Long non-coding RNA lung cancer-associated transcript 1 regulates ferroptosis via microRNA-34a-5p-mediated GTP cyclohydrolase 1 downregulation in lung cancer cells

FUMIN TAI, RUI ZHAI, KEXIN DING, YAOCANG ZHANG, HEXI YANG, HUJIE LI, QIONG WANG, ZHENGYUE CAO, CHANGHUI GE, HANJIANG FU, FENGJUN XIAO and XIAOFEI ZHENG

Department of Experimental Hematology and Biochemistry, Beijing Key Laboratory for Radiobiology, Beijing Institute of Radiation Medicine, Beijing 100850, P.R. China

Received December 27, 2023; Accepted April 9, 2024

DOI: 10.3892/ijo.2024.5652

Abstract. Ferroptosis, a recently discovered type of programmed cell death triggered by excessive accumulation of iron-dependent lipid peroxidation, is linked to several malignancies, including non-small cell lung cancer. Long non-coding RNAs (lncRNAs) are involved in ferroptosis; however, data on their role and mechanism in cancer therapy remains limited. Therefore, the aim of the present study was to identify ferroptosis-associated mRNAs and lncRNAs in A549 lung cancer cells treated with RAS-selective lethal 3 (RSL3) and ferrostatin-1 (Fer-1) using RNA sequencing. The results demonstrated that lncRNA lung cancer-associated transcript 1 (LUCAT1) was significantly upregulated in lung adenocarcinoma and lung squamous cell carcinoma tissues. Co-expression analysis of differentially expressed mRNAs and lncRNAs suggested that LUCAT1 has a crucial role in ferroptosis. LUCAT1 expression was markedly elevated in A549 cells treated with RSL3, which was prevented by co-incubation with Fer-1. Functionally, overexpression of LUCAT1 facilitated cell proliferation and reduced the occurrence of ferroptosis induced by RSL3 and Erastin, while inhibition of LUCAT1 expression reduced cell proliferation and increased ferroptosis. Mechanistically, downregulation of LUCAT1 resulted in the downregulation of both GTP cyclohydrolase 1 (GCH1) and ferroptosis suppressor protein 1 (FSP1). Furthermore, inhibition of LUCAT1 expression upregulated microRNA (miR)-34a-5p and then downregulated GCH1. These results indicated that inhibition of LUCAT1 expression promoted ferroptosis by modulating the downregulation of GCH1, mediated by miR-34a-5p. Therefore, the combination of knocking down LUCAT1 expression with ferroptosis inducers may be a promising strategy for lung cancer treatment.

Correspondence to: Professor Xiaofei Zheng or Professor Fengjun Xiao, Department of Experimental Hematology and Biochemistry, Beijing Key Laboratory for Radiobiology, Beijing Institute of Radiation Medicine, 27 Taiping Road, Beijing 100850, P.R. China
E-mail: xfzheng100@126.com
E-mail: xiaofjun@sina.com

Abbreviations: BP, Biological Process; DHODH, dihydroorotate dehydrogenase; Fer-1, ferrostatin-1; FSP1, ferroptosis suppressor protein 1; GAPDH, glyceraldehyde-3-phosphate dehydrogenase; GCH1, GTP cyclohydrolase 1; GO, Gene Ontology; GPX4, glutathione peroxidase 4; KEGG, Kyoto Encyclopedia of Genes and Genomes; lncRNA, long non-coding RNA; LUCAT1, lung cancer-associated transcript 1; miRNA, microRNA; NSCLC, non-small cell lung cancer; PPI, protein-protein interaction; RSL3, RAS-selective lethal 3

Key words: lung cancer-associated transcript 1, microRNA-34a-5p, GTP cyclohydrolase 1, ferroptosis, lung cancer

Introduction

Ferroptosis, first defined by Dixon *et al* (1) in 2012, is a relatively novel type of programmed cell death distinguished from apoptosis, necroptosis and pyroptosis by the presence of smaller mitochondria and a reduced number of mitochondrial cristae. Ferroptosis was initially explored in mammalian systems and is now known as one of the most prevalent forms of cell death (2). Ferroptosis is driven by lethal lipid peroxidation resulting from unbalanced redox homeostasis and cellular metabolism, which is inhibited by antioxidant systems, mainly including the glutathione peroxidase 4 (GPX4)-glutathione (3), ferroptosis suppressor protein 1 (FSP1)-CoQH2 (4,5), GTP cyclohydrolase 1 (GCH1)-tetrahydrobiopterin (6) and dihydroorotate dehydrogenase (DHODH)-CoQH2 systems (7). RAS-selective lethal 3 (RSL3) and Erastin are two small-molecule RSL compounds that induce ferroptosis, which is inhibited by ferrostatin-1 (Fer-1). RSL3 directly inactivates GPX4, inhibiting its ability to convert lipid hydroperoxides to lipid alcohols and triggering ferroptosis, whereas Erastin suppresses system Xc^-, decreasing cystine uptake and enhancing the levels of reactive oxygen species (ROS) (1,8,9). Fer-1 is thought to have antioxidant abilities as it scavenges alkoxyl radicals and other rearrangement products generated by ferrous iron from lipid hydroperoxides (10). Dixon *et al* (1) found that Fer-1 specifically inhibited ferroptosis induced by RSL but not the other known forms of cell death. Various

signalling pathways, such as the p53 and PI3K/AKT/mTOR signalling pathways, linked to cancer regulate ferroptosis in cancer cells, and accumulating evidence suggests that ferroptosis has an essential role in cancer progression (11,12).

Long non-coding RNAs (lncRNAs), defined as non-coding transcripts with sequences >200 nucleotides, are involved in gene expression regulation in diverse biological processes, including as RNA decoys (13), microRNA (miRNA) sponges (14) and scaffolds (15). lncRNAs have important roles as tumour suppressors or oncogenes, influencing the emergence of cancer (16). Recently, RNA sequencing (RNA-Seq) and bioinformatics analyses have demonstrated the involvement of certain lncRNAs in ferroptosis. For instance, H19 has an important role in ferroptosis caused by curcumenol by regulating miR-19b-3p-mediated ferritin heavy chain 1 (FTH1) downregulation (17). Moreover, Qin *et al* (18) constructed a 5-lncRNA (AC055720.2, LINC00900, DPP4-DT, LINC02454 and AC012038.2) signature related to ferroptosis to predict thyroid cancer prognosis and immune responses. Nevertheless, the function and regulatory mechanisms of lncRNAs associated with ferroptosis in cancer have not yet been fully investigated.

Lung cancer-associated transcript 1 (LUCAT1) was first identified in the airways of patients with a history of smoking; hence, it is sometimes referred to as smoke and cancer-associated lncRNA-1 (19). LUCAT1 expression is essential for tumour-node-metastasis staging and overall survival predictions for several malignancies, including liver cancer (20), gastric cancer (21), colorectal cancer (22,23) and renal cell carcinoma (24). Previous bioinformatics data have indicated that LUCAT1 is a ferroptosis-related lncRNA that can be used in prognostic or diagnostic signatures in renal cell carcinoma (25,26) and glioma (27). However, to the best of our knowledge, the role of LUCAT1 in lung cancer ferroptosis and its underlying mechanisms remain unknown.

Therefore, the aim of the present study was to identify ferroptosis-related lncRNAs and investigate their roles and regulatory mechanisms in lung cancer. Lung cancer cells were treated with the ferroptosis inducer, RSL3, and inhibitor, Fer-1, and ferroptosis-associated lncRNAs were identified by RNA-Seq. Investigating the functions of these lncRNAs in ferroptosis offers a novel theoretical foundation for therapeutic strategies in lung cancer.

Materials and methods

Cell culture. The human normal lung epithelial cell line, BEAS-2B (cat. no. HTX2075), was obtained from Otwo Biotech (Shenzhen Haodihuatuo Biotechnology Co., Ltd.). The lung cancer cell line, A549 (cat. no. CCL-185), and the 293T cell line (cat. no. CRL-11268) were obtained from the American Type Culture Collection. The lung cancer cell line, H460 (cat. no. CL-0299), was obtained from Procell Life Science & Technology Co., Ltd. All cell lines were authenticated by their suppliers through STR profiling. The A549, BEAS-2B, and 293T cells were cultured in DMEM (Gibco; Thermo Fisher Scientific, Inc.) with 10% foetal bovine serum (Gemini Bio Products), 100 U/ml penicillin and 100 μg/ml streptomycin at 37˚C with 5% CO_2. H460 cells were cultured in RPMI-1640 medium (Gibco; Thermo Fisher Scientific, Inc.) with the same supplements and conditions.

RNA-Seq. A549 cells were treated in triplicate with 0.7% dimethyl sulfoxide (DMSO; solvent used to dissolve RSL3 and Fer-1), 2 μM RSL3 (28) (cat. no. HY-100218A; MedChemExpress), or 2 μM RSL3 and 5 μM Fer-1 (29) (cat. no. S7243; Selleck Chemicals) for 24 h. Total RNA was extracted using TRIzol reagent (cat. no. T9424; Sigma-Aldrich; Merck KGaA), and the quantity and purity of the extracted RNA were analysed using an RNA 6000 Nano LabChip Kit (cat. no. 5067-1511; Agilent Technologies, Inc.) by Bioanalyzer 2100 (Agilent Technologies, Inc.). The 2x 150 bp paired-end sequencing was performed using an Illumina Novaseq™ 6000 at LC-Bio Technology (Hangzhou) Co., Ltd.

Bioinformatics analysis. Using genes from the aforementioned 9 samples with a mean fragments per kilobase of transcript per million mapped reads value >1, differentially expressed genes (DEGs) between the treatment and control samples were identified using DEseq2 software (version 1.40.2; https://github.com/mikelove/DESeq2), based on fold change >1.5 and $P<0.05$ as the cut-off. Biological Process (BP) of Gene Ontology (GO) and Kyoto Encyclopedia of Genes and Genomes (KEGG) pathway analyses of the DEGs were performed using Metascape (https://metascape.org/gp) (30). Heatmaps, volcano plots and Venn diagrams were created using OmicStudio (https://www.omicstudio.cn). Protein-protein interaction (PPI) networks were examined using STRING (https://www.string-db.org/). The co-expression analysis of mRNA-lncRNA was performed using the online resource, weishengxin (https://www.bioinformatics.com.cn). GO analysis of LUCAT1 and the prediction of target genes of DElncRNAs was performed using LncACTdb 3.0 (http://bio-bigdata. hrbmu.edu.cn/LncACTdb) (31). Expression specificity analysis of mRNA and lncRNA was conducted using index τ, following the method described by Li *et al* (32). The location of LUCAT1 was predicted using lncLocator (http://www.csbio.sjtu.edu.cn/bioinf/lncLocator2/) (33). LUCAT1 data were obtained from the GEO database (https://www.ncbi.nlm.nih.gov/geo/) [accession nos. GSE104462 (34) and GSE158458 (35)] and were associated with liver cancer lines (including HepG2, Hep3B and Huh7). Potential miRNAs targeting LUCAT1 or the 3'-untranslated region (3'-UTR) of GCH1 were predicted using DIANA-LncBase v3 (https://diana.e-ce.uth.gr/lncbasev3/interactions) (36) or TargetScan (http://www.targetscan.org). miR-34a-5p and LUCAT1 or GCH1 binding sites were predicted using miRDB (http://www.mirdb.org) (37) or TargetScan. Pan-cancer data were downloaded from the UCSC Xena Pan-Cancer Atlas Hub (https://xenabrowser.net/datapages/), and the expression of lncRNAs were analysed using R software (version 4.2.2; https://cran.r-project.org/src/base/R-4/).

Plasmid, stable cell line generation, small interfering RNA (siRNA), miRNA mimics and miRNA inhibitors transfections. The LUCAT1-expression vector was constructed using the PB-CMV-MCS-EF1α-RedPuro vector (cat. no. PB514B-2; System Biosciences, LLC) by YouBio. A549 cells in 6-well plates were co-transfected with 0.5 μg LUCAT1-expression vector (LUCAT1) or its control (Vector) and 0.2 μg Super PiggyBac Transposase Expression Vector (cat. no. PB210PA-1; System Biosciences, LLC) using the jetPRIME transfection

reagent (cat. no. 101000046; Polyplus-transfection SA) at room temperature, and cells that stably expressed LUCAT1 were selected using 2 μg/ml puromycin (cat. no. A1113803; Gibco; Thermo Fisher Scientific, Inc.) and subsequently maintained with 1 μg/ml puromycin. LUCAT1 siRNA (siLUCAT1) and its control (siNC), mimics of miR-34a-5p (miR-34a-5p) and its control (miR-NC), and inhibitors of miR-34a-5p (anti-miR-34a-5p) and its control (anti-NC), synthesised by Genepharm, Inc., were transfected into H460 cells at a final concentration of 50 nM under the same conditions as aforementioned. The sequences used in these experiments are shown in Table SI. The gene RNA expression level was detected 48 h after transfection, and the protein expression level was detected 72 h after transfection.

Cell viability assay. The viability of cells was assessed using Cell Counting Kit-8 (CCK-8; cat. no. CK04; Dojindo Molecular Technologies, Inc.). To measure cell proliferation, cells were seeded at a density of $1x10^3$ cells/well into 96-well plates and cultured for 0, 24, 48 and 72 h. To measure cytotoxicity, cells were seeded at a density of $5x10^3$ cells/well into 96-well plates, cultured overnight and treated with RSL3 and Erastin (A549 cells were treated with 2 μM RSL3 or 20 μM Erastin and H460 cells were treated with 8 μM RSL3 or 20 μM Erastin) for 24 h. After adding the mixture (CCK-8 reagent: medium, 1:10) into the wells and incubating at 37˚C for 1 h, a microplate reader (LabSystems Multiskan MS; Thermo Fisher Scientific, Inc.) was used to measure the absorbance at 450 nm.

Colony formation assay. Cells were seeded at a density of $1x10^3$ cells/well into 6-well plates, cultured overnight and treated with RSL3 or Erastin (A549 cells were treated with 0.1 μM RSL3 or 4 μM Erastin and H460 cells were treated with 2 μM RSL3 or 4 μM Erastin) for 10 days. After 20 min of methanol fixation at room temperature, 0.2% crystal violet was used to stain the cells for 5 min at room temperature. ImageJ software (version 1.53a; National Institutes of Health) was used to count colonies with >50 cells, and analysis was performed using GraphPad Prism (version 9.0; Dotmatics).

Lipid ROS assay. Lipid ROS was detected using a BODIPY 581/591 C11 Kit (cat. no. D3861; Invitrogen; Thermo Fisher Scientific, Inc.). Cells were seeded at a density of $1.5x10^5$ cells/well into 6-well plates, cultured overnight and treated with RSL3 or Erastin (A549 cells were treated with 2 μM RSL3 or 20 μM Erastin and H460 cells were treated with 8 μM RSL3 or 20 μM Erastin) at 37˚C for 24 h. Subsequently, the cells were harvested and stained with 2 μM C11-BODIPY (581/591) probe at 37˚C for 30 min in the dark. At least $1x10^4$ cells were collected to measure the fluorescence using the BD FACSAria™ II flow cytometer (BD Biosciences). FlowJo V10 software (FlowJo, LLC) was used to analyse the data.

Reverse transcription-quantitative PCR (RT-qPCR). TRIzol reagent was used to extract the total RNA, and the extracted RNA was reverse transcribed into cDNA using an ImProm-II™ Reverse Transcriptase Reagent Kit (cat. no. A3803; Promega Corporation) according to the manufacturer's instructions. qPCR was performed in a Mx3000P instrument (Agilent Technologies, Inc.) using PowerUp™ SYBR™ Green Master Mix (cat. no. A24742; Applied Biosystems; Thermo Fisher Scientific, Inc.). For detecting miRNA expression, poly(A) tails were added before RT using *E. coli* poly(A) polymerase (cat. no. M0276S; New England BioLabs, Inc.). The qPCR conditions were as follows: i) 50˚C for 2 min; ii) 95˚C for 2 min; and iii) 40 cycles of 95˚C for 5 sec and 60˚C for 30 sec. To normalise the levels of miRNA expression and other genes, U6 or glyceraldehyde-3-phosphate dehydrogenase (GAPDH) RNA were utilised, and the relative gene expression levels were calculated using the $2^{-\Delta\Delta Cq}$ method (38). Table SII depicts the RT-qPCR primer sequences used in this assay.

Western blotting. RIPA Lysis Buffer (cat. no. ZE122-101S; Genstar Biosolutions Co., Ltd.) containing Protease Inhibitor Cocktail (cat. no. B14001; Bimake) was used to extract the total proteins from cells. The Pierce™ BCA Protein Assay Kit (cat. no. 23227; Thermo Fisher Scientific, Inc.) was utilised to quantify protein concentrations in the samples. Then, samples with 15 μg of protein were separated via 12% SDS-PAGE gels and transferred to nitrocellulose membranes (cat. no. 66485; Pall Life Sciences). After blocking the membrane with 5% non-fat milk at room temperature for 1 h, the membranes were incubated with primary antibodies overnight at 4˚C. The following primary antibodies were used: GAPDH (1:20,000; cat. no. 60004-1-Ig; ProteinTech Group, Inc.); GCH1 (1:2,000; cat. no. 28501-1-AP; ProteinTech Group, Inc.); GPX4 (1:5,000; cat. no. ab125066; Abcam) and FSP1 (1:2,000; cat. no. 20886-1-AP; ProteinTech Group, Inc.). Then, the membranes were incubated with secondary antibodies at room temperature for 1 h. The secondary antibodies used were as follows: Goat anti-mouse (1:5,000; cat. no. SA00001-1; ProteinTech Group, Inc.) and goat anti-rabbit (1:5,000; cat. no. SA00001-2; ProteinTech Group, Inc.). The signals were visualised using HRP Substrate Luminol Reagent (cat. no. WBKLS0500; MilliporeSigma) and imaged using a chemiluminescence imaging system (Tanon-4600SF; Tanon Science and Technology Co., Ltd.). ImageJ software was used for the semi-quantitation of protein.

Dual-luciferase reporter assay. Full-length LUCAT1 was inserted into the pGL3-basic vector (Promega Corporation) using *Xba*I and *Nde*I (cat. nos. R0145S and R0111S; New England BioLabs, Inc.) to create the LUCAT1 reporter vector. The GCH1 3'-UTR reporter vector was also constructed by insertion into the pGL3-basic vector. Using the QuickMutation™ Plus Kit (cat. no. D0208S; Beyotime Institute of Biotechnology), the binding sites 'CACUGCC' (position 869-875 in LUCAT1 or position 255-261 in the GCH1 3'-UTR) were changed to 'GCGACGG' to create mutated variants of the LUCAT1 and the GCH1 3'-UTR reporter vector. Dual-luciferase reporter assays were conducted by co-transfecting 293T cells with the *Renilla* Luciferase Expression Vector (Promega Corporation), the LUCAT1 or GCH1 3'-UTR reporter vector, and miR-NC or miR-34a-5p mimics using jetPRIME transfection reagent. After 48 h of transfection, the cells were lysed by the Dual-Luciferase Reporter Assay System (cat. no. E1910; Promega Corporation),

and the luciferase activities were measured by GloMax® 20/20 Luminometer (Promega Corporation). Transfection efficiencies were standardised using *Renilla* luciferase. Table SIII shows the sequences of the primers used in this assay.

Statistical analysis. The data are presented as the mean ± SD. Unpaired Student's t-test (two-tailed) and one-way analysis of variance (ANOVA) or two-way ANOVA followed by Tukey's test were used to analyse the differences between the different groups, using GraphPad Prism software. $P<0.05$ was used to indicate a statistically significant difference.

Results

Identification of DEmRNAs involved in regulating ferroptosis. To identify genes involved in ferroptosis, A549 cells were treated with DMSO, RSL3 or RSL3 + Fer-1. RSL3 (2 μM) inhibited approximately half of the cell viability of A549 cells, which was prevented by co-incubation with 5 μM Fer-1 (Fig. S1). Subsequently, RNA-Seq was performed. When comparing the RSL3 treatment group with the DMSO group, 291 DEmRNAs were identified, including the ferroptosis-related genes, solute carrier family 7 member 11, prostaglandin-endoperoxide synthase 2, FTH1, heme oxygenase 1 and TP53 (1,39-42) (Fig. 1A and B), of which 82 were rescued (expression level was restored) by co-incubation with Fer-1, indicating that these 82 DEmRNAs may be important for ferroptosis (Fig. 1C). The DEmRNAs were enriched in the BP terms, 'response to oxygen levels' and 'positive control of programmed cell death' (Fig. 1D). KEGG pathway analysis revealed that the ferroptosis-related, 'HIF-1 signaling pathway' (43), and 'TNF signaling pathway' (44) were also enriched during ferroptosis (Fig. 1E). Among the top 10 hub mRNAs in the PPI network displayed using STRING, jun proto-oncogene, C-X-C motif chemokine ligand 8, epiregulin, cyclin-dependent kinase inhibitor 1A, serpin family E member 1 and DNA damage-inducible transcript 3 were previously reported to be involved in ferroptosis (45-50), suggesting that the remaining four genes, growth arrest and DNA damage inducible α (GADD45A), epithelial mitogen (EPGN), heparin-binding EGF-like growth factor (HBEGF) and transforming growth factor α (TGFA), may also have roles in ferroptosis (Fig. 1F and G). These results therefore identified novel genes that may be involved in ferroptosis caused by alkoxyl radicals and other rearrangement products generated by ferrous iron from lipid hydroperoxides.

LUCAT1 is upregulated in RSL3-induced ferroptosis, which is prevented by co-incubation with Fer-1. In addition to the 82 DEmRNAs, 18 DElncRNAs were either upregulated or downregulated in the RSL3 group compared with the DMSO group, which was prevented by co-incubation with Fer-1 (Fig. 2A-D). The genes targeted by DElncRNAs were enriched in the BP terms 'regulation of growth' and 'response to oxygen levels' (Fig. 2E). Additionally, KEGG pathway analysis revealed that the 'MAPK signaling pathway' (51,52), 'Hippo signaling pathway' (53) and 'Wnt signaling pathway' (54) were enriched (Fig. 2F), suggesting that DElncRNAs are involved in ferroptosis.

Compared with mRNA expression levels, the global expression level of lncRNA was much lower (Fig. 2G). However, the lncRNAs displayed a greater degree of expression specificity compared with that of the mRNAs (Fig. 2H). To identify lncRNAs that were more important in ferroptosis, their correlations with DEmRNAs were examined and mRNA-lncRNA co-expression networks were constructed. Using a robust correlation ($|r|>0.9$, $P<0.05$) as the cut-off for mRNA-lncRNA pairs, 93 nodes (16 DElncRNAs and 77 DEmRNAs) and 589 mRNA-lncRNA pairs (544 with a positive correlation and 45 with a negative correlation) were identified. The mRNA-lncRNA pairs with the top 100 correlation coefficients ($|r|$) were used for network construction (Fig. 2I).

Among the 18 DElncRNAs, LUCAT1 was the most highly upregulated, ranking first among the candidates (Fig. 2J), and it had an important role in the constructed mRNA-lncRNA co-expression network (Fig. 2I). Therefore, it was next confirmed that LUCAT1 was upregulated following treatment with RSL3 and prevented by co-incubation with Fer-1 (Fig. 2K and L). After treating A549 cells with RSL3, LUCAT1 expression increased in a dose-dependent manner and maximum LUCAT1 expression occurred after 12 h of treatment with 4 μM RSL3 (Fig. 2M and N). To obtain more evidence for the connection between LUCAT1 and ferroptosis, the GEO database was utilised to explore the relationship between LUCAT1 and other ferroptosis inducers in cancer. It was found that LUCAT1 was elevated in HepG2 liver cancer cells treated with Erastin and in two sorafenib-resistant liver cancer lines (Hep3B and Huh7) by bioinformatic analysis (Fig. S2A-C), suggesting that ferroptosis inducer-induced upregulation of LUCAT1 may be common in different types of cancer. Furthermore, the top three GO terms for LUCAT1 predicted by the LncACTdb were 'superoxide metabolic process' (55), 'MAPK activity' (51,52) and 'oxygen and reactive oxygen species metabolic process' (56), which all have important roles in ferroptosis (Fig. 2O). These results reflected a possible close relationship between ferroptosis and LUCAT1.

Genes that are expressed at either high or low levels in tumours influence the growth and treatment of the tumours (57). LUCAT1 expression was higher in 18 different types of cancer tissues than in the corresponding normal tissues (Fig. S3A). Compared with normal tissues, LUCAT1 expression was higher in lung adenocarcinoma and lung squamous cell carcinoma (Fig. S3B and C). Similarly, two lung cancer cell lines, A549 and H460, expressed higher levels of LUCAT1 compared with the BEAS-2B normal lung epithelial cell line (Fig. S3D). These findings suggested that LUCAT1 functions as an oncogene in lung cancer.

LUCAT1 overexpression inhibits RSL3- and Erastin-induced ferroptosis. The expression of LUCAT1 was lower in A549 cells than in H460 cells (Fig. S3D); therefore, the effect of overexpressing LUCAT1 in A549 cells was examined (Fig. 3A). As shown in Fig. 3B, LUCAT1 overexpression significantly enhanced A549 cell proliferation. When ferroptosis was induced by RSL3 and Erastin, overexpression of LUCAT1 enhanced the survival rate and colony formation of A549 cells (Fig. 3C and D). Similarly, lipid peroxidation levels were elevated by RSL3 and Erastin treatment; however, LUCAT1 overexpression reduced these levels (Fig. 3E). Collectively,

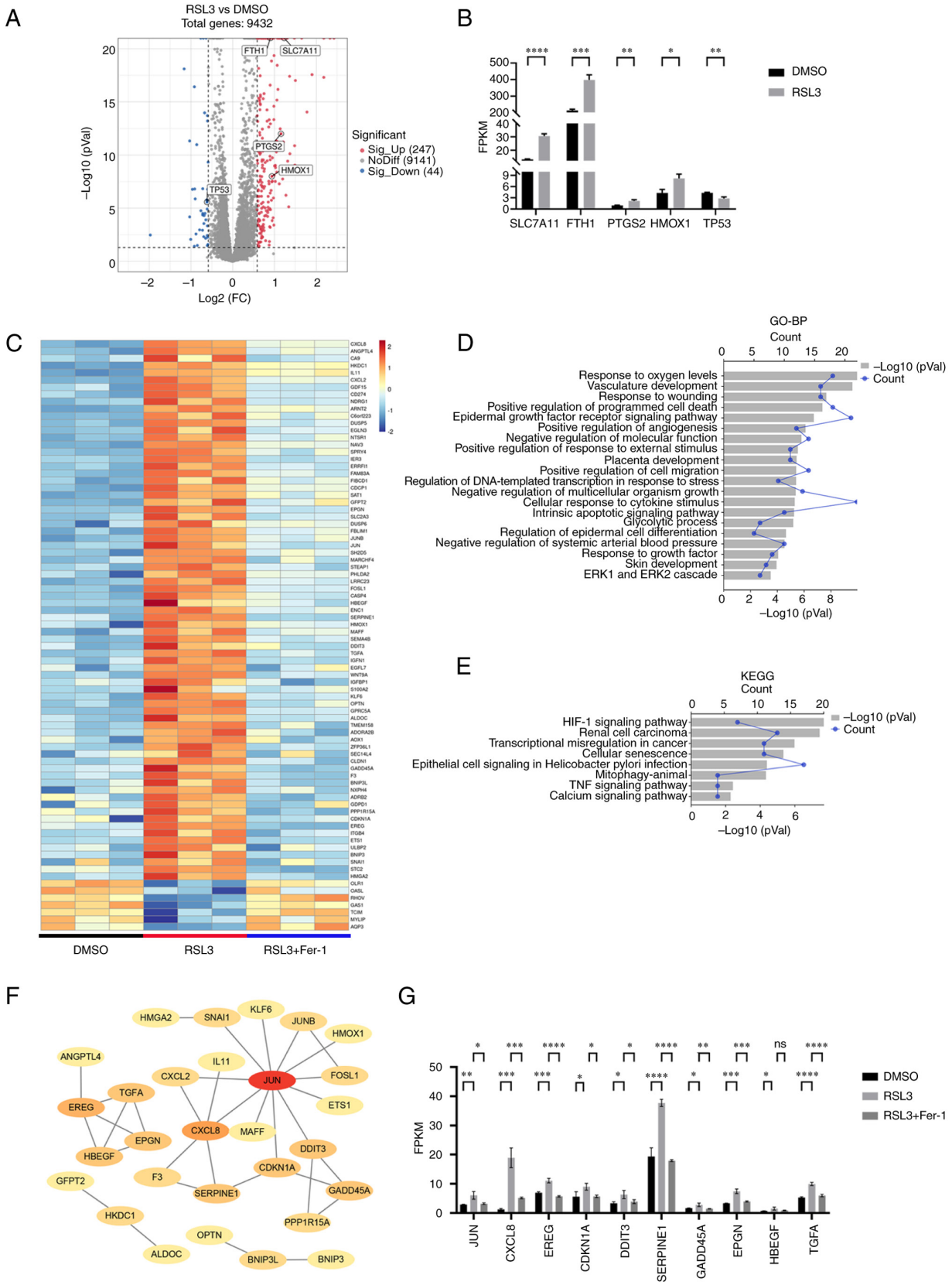

Figure 1. Expression profiles of mRNAs in ferroptosis. (A) Volcano plot for the RSL3 group vs. the DMSO group. (B) The FPKM value of ferroptosis-associated genes in the DMSO and RSL3 groups. (C) Heatmap showing the overlap of 82 DEmRNAs between the RSL3 vs. DMSO groups and the RSL3 vs. RSL3 + Fer-1 groups. (D) Top 20 GO-BP terms for the DEmRNAs. (E) KEGG terms for the DEmRNAs. (F) PPI network of DEmRNAs. (G) The FPKM value of the top 10 hub genes in the PPI network. *P<0.05, **P<0.01, ***P<0.001, ****P<0.0001. RSL3, RAS-selective lethal 3; DEmRNAs, differentially expressed mRNAs; Fer-1, ferrostatin-1; GO, Gene Ontology; BP, Biological Process; KEGG, Kyoto Encyclopedia of Genes and Genomes; PPI, protein-protein interaction; FPKM, fragments per kilobase of transcript per million mapped reads; FC, fold change; ns, not significant; SLC7A11, solute carrier family 7 member 11; FTH1, ferritin heavy chain 1; PTGS2, prostaglandin-endoperoxide synthase 2; HMOX1, heme oxygenase 1; JUN, jun proto-oncogene; CXCL8, C-X-C motif chemokine ligand 8; EREG, epiregulin; CDKN1A, cyclin-dependent kinase inhibitor 1A; DDIT3, DNA damage-inducible transcript 3; GADD45A, growth arrest and DNA damage inducible α; HBEGF, heparin-binding EGF-like growth factor.

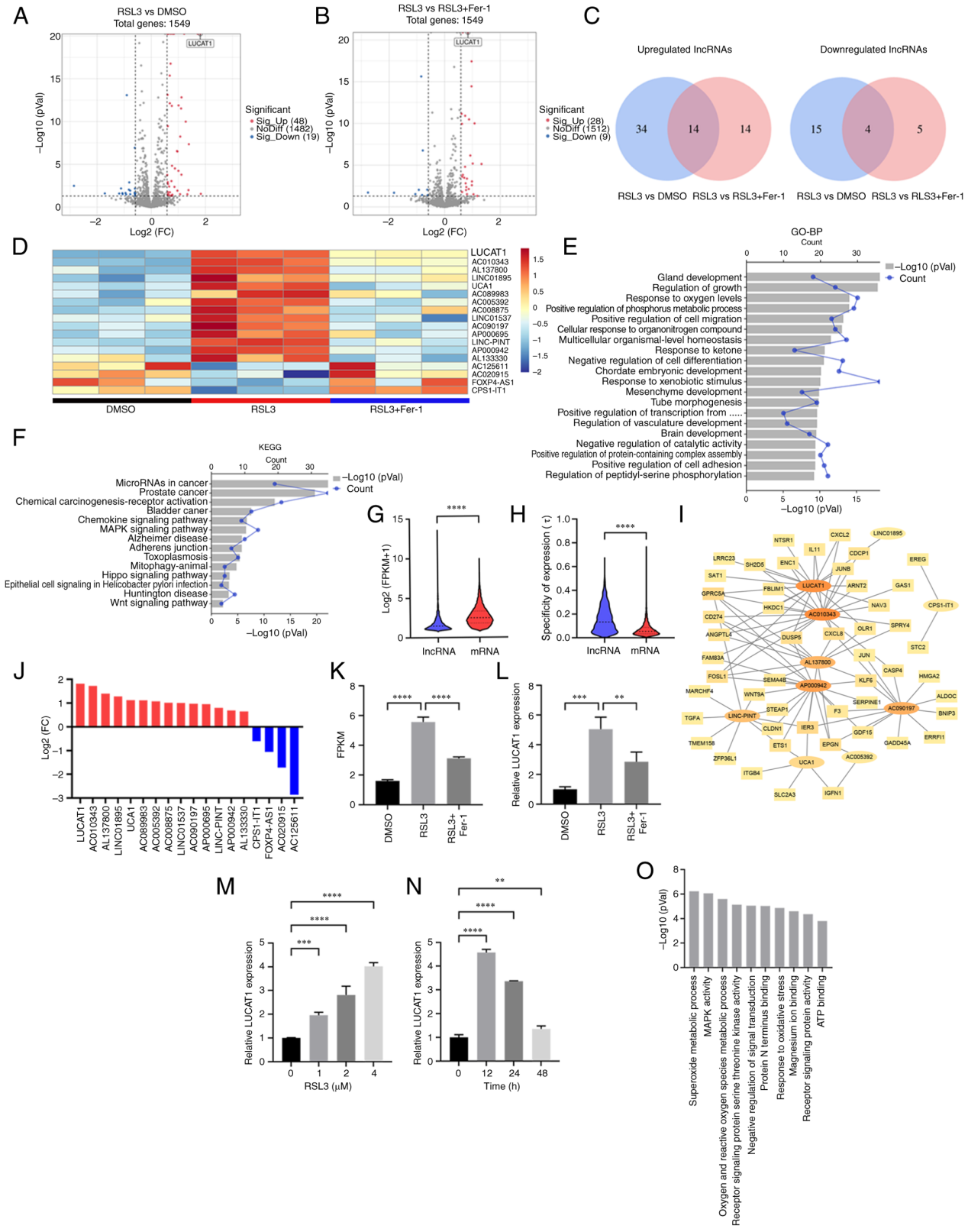

Figure 2. LUCAT1 is upregulated in RSL3-induced ferroptosis, which is inhibited by Fer-1. (A) Volcano map for the RSL3 vs. DMSO group. (B) Volcano map for the RSL3 vs. RSL3 + Fer-1 group. (C) The overlap of the DElncRNAs between the RSL3 vs. DMSO group and the RSL3 vs. RSL3 + Fer-1 group. (D) Heatmap of the 18 DE lncRNAs. (E) Top 20 GO-BP terms enriched for the target genes of DElncRNAs. (F) KEGG terms enriched for the target genes of the DElncRNAs. (G) Log_2 (FPKM+1) of lncRNAs and mRNAs. (H) Specific expression analysis of lncRNAs and mRNAs. (I) Co-expression networks between DElncRNAs and DEmRNAs. (J) DElncRNAs ranked in terms of their log_2 FC values. (K) The FPKM value for LUCAT1 was determined using RNA sequencing. (L) LUCAT1 expression in the DMSO, RSL3 and RSL3 + Fer-1 groups was detected using RT-qPCR. (M) LUCAT1 expression in A549 cells treated with 0, 1, 2 or 4 μM RSL3 for 24 h was detected using RT-qPCR. (N) LUCAT1 expression in A549 cells treated with 4 μM RSL3 for 0, 12, 24 or 48 h was detected using RT-qPCR. (O) GO analysis of LUCAT1 was predicted using LncACTdb. **P<0.01, ***P<0.001, ****P<0.0001. All experiments were repeated three times. LUCAT1, lung cancer-associated transcript 1; RSL3, RAS-selective lethal 3; Fer-1, ferrostatin-1; DE, differentially expressed; lncRNA, long non-coding RNA; GO, Gene Ontology; BP, Biological Process; KEGG, Kyoto Encyclopedia of Genes and Genomes; FC, fold change; FPKM, fragments per kilobase of transcript per million mapped reads; RT-qPCR, reverse transcription-quantitative PCR.

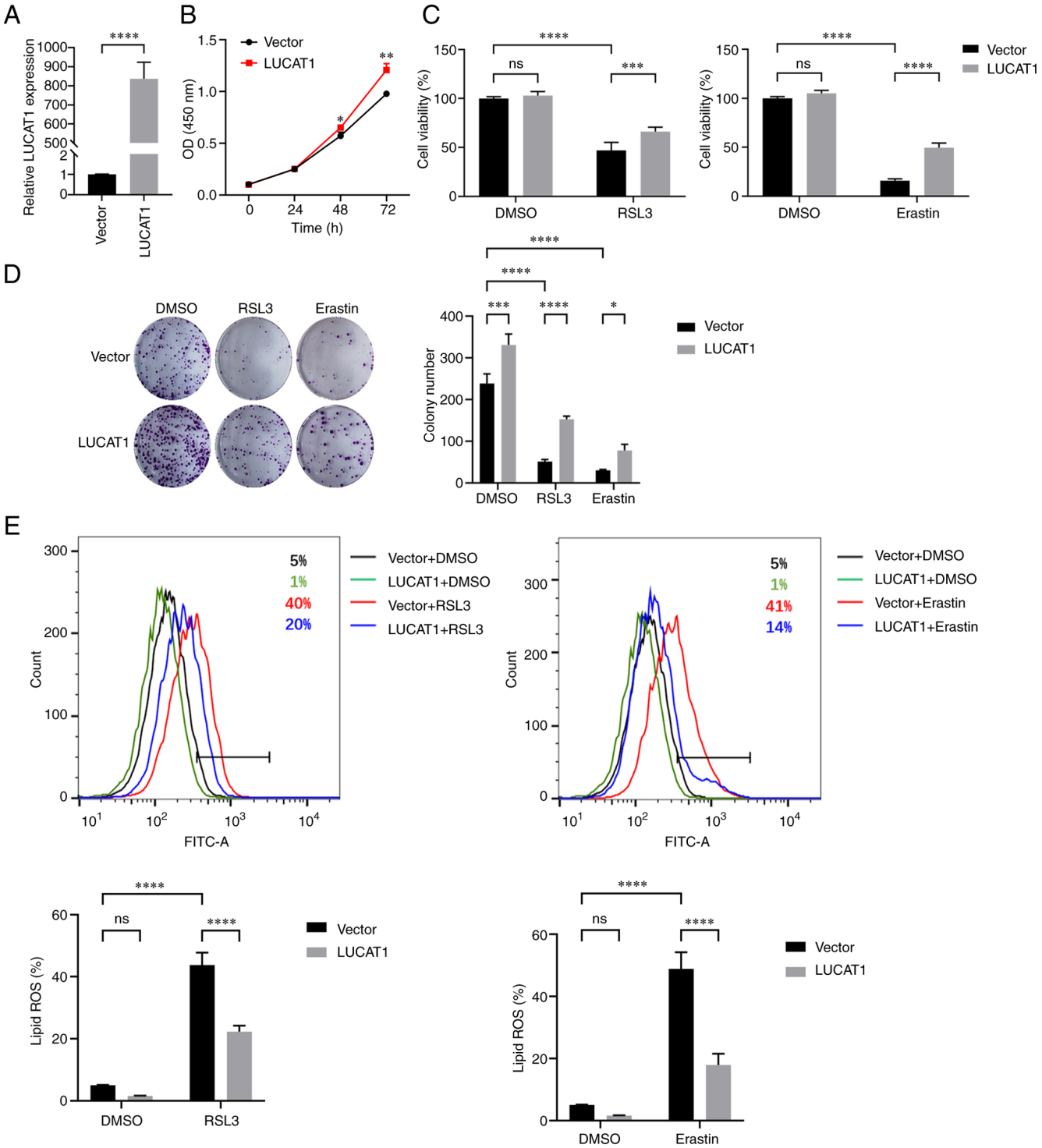

Figure 3. LUCAT1 overexpression inhibits RSL3- and Erastin-induced ferroptosis. (A) LUCAT1 expression in A549 cells was detected using reverse transcription-quantitative PCR. (B) The effect of LUCAT1 overexpression on cell proliferation was detected by CCK-8. (C) A549 cells were treated with 2 μM RSL3 or 20 μM Erastin for 24 h and the cell viability was determined using CCK-8. (D) Colony formation assay was performed following treatment with 0.1 μM RSL3 or 4 μM Erastin. (E) The histograms of lipid ROS for A549 cells treated with 2 μM RSL3 or 20 μM Erastin for 24 h. *P<0.05, **P<0.01, ***P<0.001, ****P<0.0001. All experiments were repeated three times. LUCAT1, lung cancer-associated transcript 1; RSL3, RAS-selective lethal 3; CCK-8, Cell Counting Kit-8; ns, not significant; ROS, reactive oxygen species.

these data suggested that LUCAT1 was a ferroptosis suppressor in A549 cells treated with RSL3 and Erastin.

Knocking down LUCAT1 expression promotes RSL3- and Erastin-induced ferroptosis. As LUCAT1 was expressed at higher levels in H460 cells than in A549 cells (Fig. S3D), the effect of knocking down LUCAT1 expression in H460 cells was next explored (Fig. 4A). Knocking down LUCAT1 expression significantly inhibited the proliferation of H460 cells (Fig. 4B). Knocking down LUCAT1 expression also significantly reduced the survival rate and colony formation capacity of H460 cells following ferroptosis induction (Fig. 4C and D).

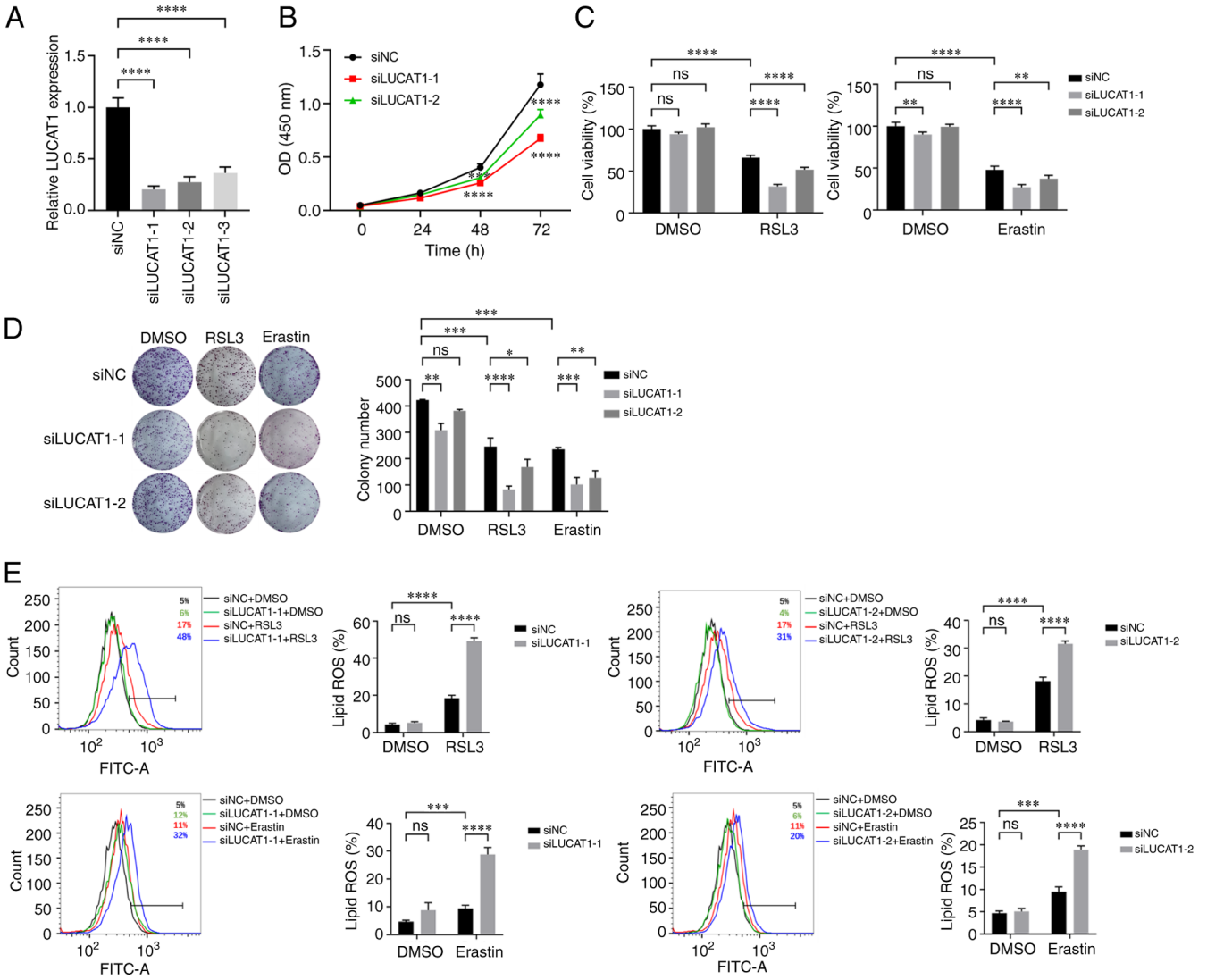

Figure 4. LUCAT1 knockdown promotes RSL3- and Erastin-induced ferroptosis. (A) LUCAT1 expression in H460 cells was detected using reverse transcription-quantitative PCR. (B) The effect of LUCAT1 knockdown on cell proliferation was detected by CCK-8. (C) H460 cells were treated with 8 μM RSL3 or 20 μM Erastin for 24 h and the cell viability was determined by CCK-8. (D) Colony formation assay was performed following treatment with 2 μM RSL3 or 4 μM Erastin. (E) The histograms of lipid ROS for H460 cells treated with 8 μM RSL3 or 20 μM Erastin for 24 h. *P<0.05, **P<0.01, ***P<0.001, ****P<0.0001. All experiments were repeated three times. LUCAT1, lung cancer-associated transcript 1; RSL3, RAS-selective lethal 3; CCK-8, Cell Counting Kit-8; ns, not significant; ROS, reactive oxygen species; si(RNA), small interfering RNA; NC, negative control.

Moreover, knocking down LUCAT1 expression increased the level of lipid peroxidation upon ferroptosis induction (Fig. 4E). These data suggested that knocking down LUCAT1 expression promoted RSL3- and Erastin-induced ferroptosis.

Knocking down LUCAT1 expression promotes ferroptosis by regulating the miR-34a-5p/GCH1 axis. To investigate the mechanism by which LUCAT1 influences ferroptosis, the expression of the main ferroptosis resistance genes were detected. FSP1 and GCH1 were downregulated in LUCAT1-knock down cells, while GPX4 expression was not affected (Fig. 5A). Owing to the greater downregulation of GCH1, we considered that LUCAT1 primarily exerted its effects through GCH1. LncLocator analysis indicated that LUCAT1 is predominantly localised in the cytoplasm (Fig. 5B); thus, it may act as a miRNA sponge in regulating GCH1 expression. Next, the shared miRNAs targeting the 3'-UTR of GCH1 (predicted by TargetScan) and LUCAT1 (predicted by DIANA-LncBase v3) were analysed and miR-34a-5p was identified as a potential mediator between the two (Fig. 5C). As illustrated in Fig. 5D, the expression level of miR-34a-5p was elevated upon LUCAT1 knockdown. Moreover, transfection with miR-34a-5p mimics downregulated GCH1 expression (Fig. 5E and F). Additionally, miR-34a-5p mimics enhanced the RSL3-induced ferroptosis sensitivity as determined via cell viability and lipid ROS assays (Fig. 5G and H). Conversely, inhibition of miR-34a-5p with anti-miR-34a-5p increased the resistance of ferroptosis mediated by LUCAT1 inhibition (Fig. 5I and J).

Using miRDB and TargetScan, the potential miR-34a-5p binding sites with LUCAT1 and the 3'-UTR of GCH1 were identified (Fig. 5K). The potential binding sites between miR-34a-5p and LUCAT1 or the 3'-UTR of GCH1 were then validated using dual-luciferase reporter assays. The luciferase activity was markedly lower in 293T cells transfected with miR-34a-5p mimics than with miR-NC; however, no changes

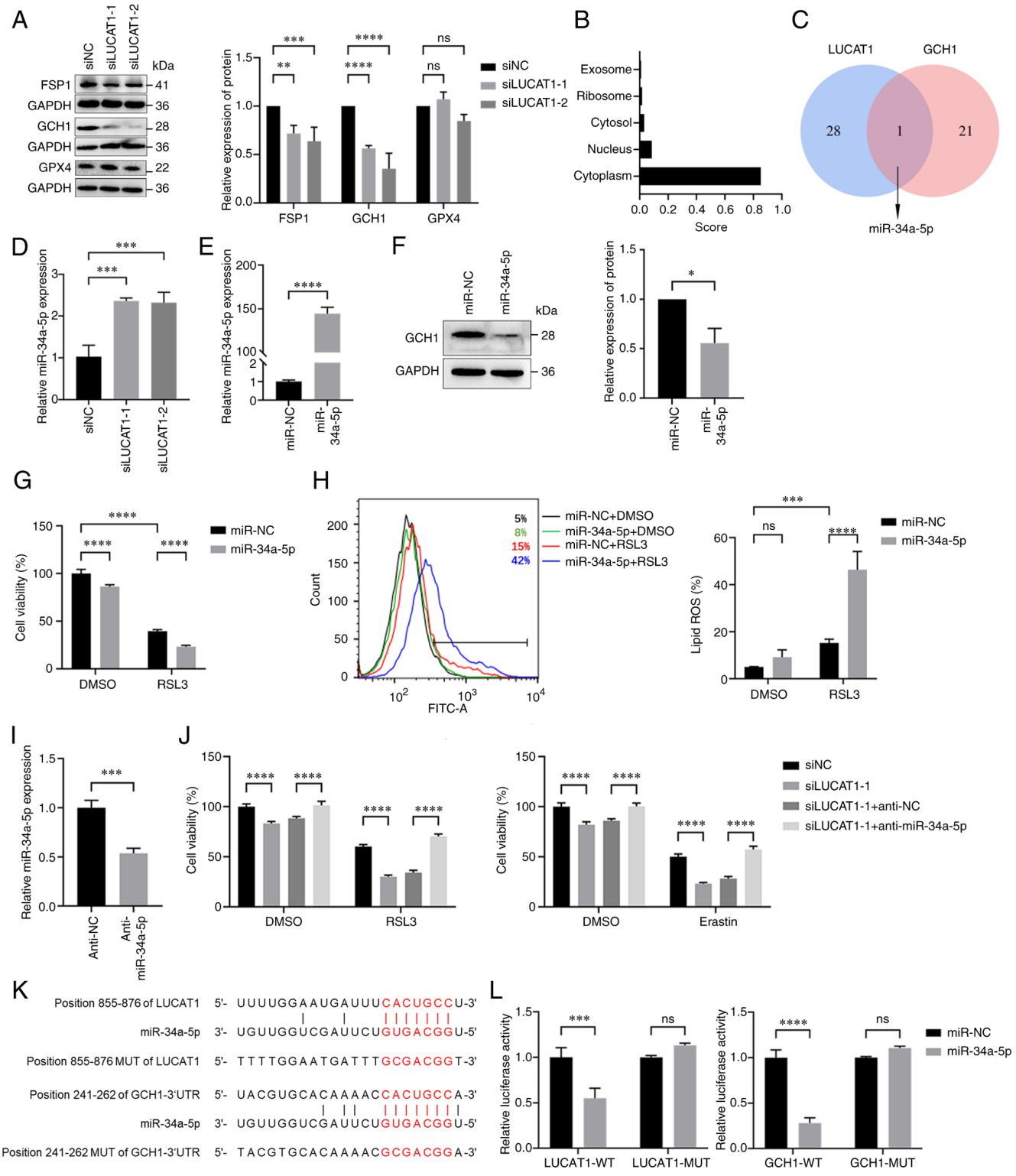

Figure 5. Knocking down LUCAT1 expression promotes ferroptosis by regulating the miR-34a-5p/GCH1 axis. (A) Expression of ferroptosis-associated proteins in H460 cells after knocking down LUCAT1 expression was detected using western blotting. (B) The subcellular localisation of LUCAT1 was predicted using lncLocator. (C) Venn diagram of overlapping miRNAs related to LUCAT1 and the 3'-UTR of GCH1. (D) miR-34a-5p expression in H460 cells after knocking down LUCAT1 expression was detected using RT-qPCR. (E) miR-34a-5p expression in H460 cells transfected with miR-34a-5p mimics was detected using RT-qPCR. (F) GCH1 protein expression in H460 cells transfected with miR-34a-5p mimics was detected using western blotting. (G) H460 cells were treated with 8 μM RSL3 for 24 h and the cell viability was determined by using CCK-8. (H) The lipid ROS histograms for H460 cells treated with 8 μM RSL3 for 24 h. (I) miR-34a-5p expression in H460 cells transfected with miR-34a-5p inhibitors was detected using RT-qPCR. (J) The viability of H460 cells treated with siNC, siLUCAT1-1, siLUCAT1-1 + anti-NC or siLUCAT1-1 + anti-miR-34a-5p groups was assessed following treatment with 8 μM RSL3 or 20 μM Erastin for 24 h using CCK-8. (K) The miR-34a-5p binding sites of LUCAT1 and 3'-UTR of GCH1 were predicted using miRDB and TargetScan. (L) Dual-luciferase reporter assays were performed to determine the associations between miR-34a-5p and LUCAT1 or GCH1. *P<0.05, **P<0.01, ***P<0.001, ****P<0.0001. All experiments were repeated three times. LUCAT1, lung cancer-associated transcript 1; GCH1, GTP cyclohydrolase 1; 3'-UTR, 3'-untranslated region; FSP1, ferroptosis suppressor protein 1; GPX4, glutathione peroxidase 4; CCK-8, Cell Counting Kit-8; RT-qPCR, reverse transcription-quantitative PCR; ns, not significant; ROS, reactive oxygen species; si(RNA), small interfering RNA; NC, negative control; miR, microRNA; GAPDH, glyceraldehyde-3-phosphate dehydrogenase; WT, wild-type; MUT, mutated.

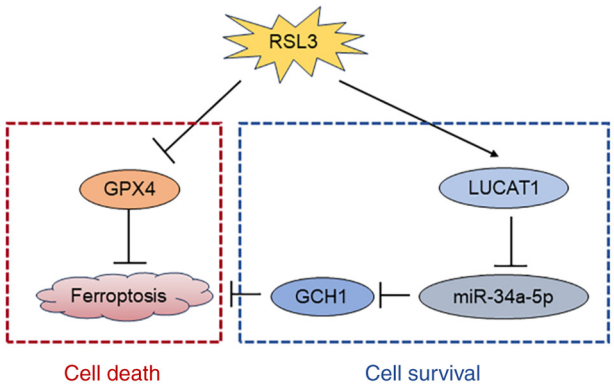

Figure 6. Proposed schematic diagram of the mechanism by which the LUCAT1/miR-34a-5p/GCH1 axis regulates ferroptosis in lung cancer cells. RSL3, RAS-selective lethal 3; GPX4, glutathione peroxidase 4; LUCAT1, lung cancer-associated transcript 1; GCH1, GTP cyclohydrolase 1; miR, microRNA.

in luciferase activity were observed in the LUCAT1-mutated (MUT) or GCH1-MUT groups (Fig. 5L). In conclusion, these findings suggested that LUCAT1 may promote ferroptosis via the miR-34a-5p/GCH1 axis.

Discussion

As ferroptosis is a targetable cancer vulnerability, more attention has been paid to the impact of ferroptosis-associated genes in recent years (12). Therefore, lncRNA expression profiles were analysed in the present study and it was discovered that LUCAT1 expression was elevated following treatment with RSL3, which was prevented by Fer-1. The results of the present study also suggested that LUCAT1 acted as a miR-34a-5p sponge and upregulated GCH1 expression, enhancing the resistance of lung cancer cells to ferroptosis and thereby promoting cell survival (Fig. 6).

Ferroptosis-associated proteins have been extensively reported, some of which have been targeted to increase the sensitivity of cancer to certain drugs (58). For instance, Mao *et al* (7) reported that DHODH is a ferroptosis suppressor, and the DHODH inhibitor, brequinar, selectively inhibited the growth of tumours with low GPX4 expression by inducing ferroptosis. In addition, the growth of the tumours with high GPX4 expression was suppressed by inducing ferroptosis following combined treatment with brequinar and the FDA-approved drug, sulfasalazine. In the present study, GADD45A, EPGN, HBEGF and TGFA were identified as potentially novel ferroptosis-related genes by analysing their mRNA expression profiles under ferroptosis conditions. Qi *et al* (59) also reported that sodium selenite inhibited cervical cancer by activating GADD45A in a ROS-dependent manner (56), which is essential for ferroptosis. Although lncRNAs are vital in biological processes, data on ferroptosis-related lncRNAs remains limited. In the present study, the analysis of mRNA and lncRNA expression profiles suggested the involvement of LUCAT1 in ferroptosis. The findings indicated that LUCAT1 was significantly upregulated in A549 cells treated with RSL3, which was prevented by Fer-1. Previous studies have reported LUCAT1 upregulation in Erastin- or sorafenib-treated liver cancer cells and in pancreatic adenocarcinoma cells subjected to cystine depletion (a ferroptosis-inducing condition) (34,35,60,61). Moreover, nuclear factor erythroid 2-related factor 2 (62), specificity protein 1 (63), signal transducer and activator of transcription 3 (64) and E74-like ETS transcription factor 1 (65) regulate LUCAT1 transcription; however, whether RSL3 controls these transcription factors to regulate LUCAT1 expression requires further exploration.

Previous reports have shown that LUCAT1 promotes tumour cell migration, invasion (63) and metastasis (66), is linked to worse outcomes (67) and has been described as a key regulator of stemness in cancer (68). Vierbuchen *et al* (69) found that LUCAT1 levels are elevated in a large cohort of patients with inflammatory disorders, underlining its key role in immune regulation. Tao *et al* (70) demonstrated that LUCAT1 prevents stem cell apoptosis and improves the efficacy of stem cell therapy for ischaemic cardiovascular disease. Reduced LUCAT1 expression promotes G0/G1 phase block of the cell cycle in several tumour cells (71-75), while high expression leads to the development of cellular resistance, for instance cisplatin resistance in non-small cell lung cancer (NSCLC) (76), methotrexate resistance in osteosarcoma (77) and camptothecin, 5-fluorouracil, adriamycin and oxaliplatin resistance in colorectal cancer (22). In the present study, LUCAT1 knockdown increased the sensitivity of lung cancer cells to ferroptosis, indicating that this method could be a novel approach to treating lung cancer.

In addition, in the present study, knocking down LUCAT1 expression inhibited the expression of GCH1, which promotes tumorigenesis in KRAS-driven lung cancer (78) and was identified as a ferroptosis suppressor in a genome-wide activation screen (6). The localisations of lncRNAs are closely associated with their functions (79). In the present study, LUCAT1 was predicted to be localised in the cytoplasm, where it may act as a miR-34a-5p sponge. miR-34a-5p has been shown to inhibit cell proliferation in lung adenocarcinoma (80) and is a driver in $CdCl_2$-induced ferroptosis (81). The findings of the present study demonstrated that miR-34a-5p inhibited GCH1 expression, which in turn promoted ferroptosis in the presence of RSL3 in lung cancer.

Although this study provides a new theoretical basis for the treatment of lung cancer, there are still some limitations. Specifically, the findings of the present study suggested that the ferroptosis inducer, RSL3, regulated LUCAT1, yet the precise regulatory mechanism remains unclear. The expression levels of LUCAT1 in lung cancer and normal tissues were determined through bioinformatics analysis; however, the lack of available clinical samples hinders further validation. Furthermore, *in vivo* experiments are necessary to substantiate the suppressive function of LUCAT1 in ferroptosis. Consequently, additional research is warranted to address these unresolved questions.

In summary, the results of the present study suggested that LUCAT1 may have a critical role in ferroptosis. Overexpression of LUCAT1 induced ferroptosis resistance to rescue cell survival in the presence of RSL3. By contrast, knocking down LUCAT1 expression enhanced susceptibility to RSL3- and Erastin-induced ferroptosis via miR-34a-5p-mediated GCH1 downregulation in NSCLC cells. Therefore, the results of the present study identified a novel pathway, the

LUCAT1/miR-34a-5p/GCH1 axis, which regulated ferroptosis sensitivity and may be targeted for the treatment of lung cancer.

Acknowledgements

Not applicable.

Funding

The present study was supported by The National Natural Science Foundation of China (grant nos. 82073489 and 32071290).

Availability of data and materials

The RNA sequencing data generated in the present study may be found in the GEO database under accession number GSE247883 or at the following URL: https://www.ncbi.nlm.nih.gov/geo/query/acc.cgi?acc=GSE247883. All other data generated in the present study may be requested from the corresponding author.

Authors' contributions

XZ, FX, HF and FT conceived and designed the experiments. FT, RZ, KD, YZ, HY, HL, QW and ZC performed the experiments. FT and CG analysed the data. FT wrote the manuscript. XZ, FX, HF and CG revised the manuscript. XZ and FT confirm the authenticity of all the raw data. All authors read and approved the final version of the manuscript.

Ethics approval and consent to participate

Not applicable.

Patient consent for publication

Not applicable.

Competing interests

The authors declare that they have no competing interests.

References

1. Dixon SJ, Lemberg KM, Lamprecht MR, Skouta R, Zaitsev EM, Gleason CE, Patel DN, Bauer AJ, Cantley AM, Yang WS, *et al*: Ferroptosis: An iron-dependent form of nonapoptotic cell death. Cell 149: 1060-1072, 2012.
2. Stockwell BR, Friedmann Angeli JP, Bayir H, Bush AI, Conrad M, Dixon SJ, Fulda S, Gascón S, Hatzios SK, Kagan VE, *et al*: Ferroptosis: A regulated cell death nexus linking metabolism, redox biology, and disease. Cell 171: 273-285, 2017.
3. Seibt TM, Proneth B and Conrad M: Role of GPX4 in ferroptosis and its pharmacological implication. Free Radic Biol Med 133: 144-152, 2019.
4. Bersuker K, Hendricks JM, Li Z, Magtanong L, Ford B, Tang PH, Roberts MA, Tong B, Maimone TJ, Zoncu R, *et al*: The CoQ oxidoreductase FSP1 acts parallel to GPX4 to inhibit ferroptosis. Nature 575: 688-692, 2019.
5. Doll S, Freitas FP, Shah R, Aldrovandi M, da Silva MC, Ingold I, Goya Grocin A, Xavier da Silva TN, Panzilius E, Scheel CH, *et al*: FSP1 is a glutathione-independent ferroptosis suppressor. Nature 575: 693-698, 2019.
6. Kraft VAN, Bezjian CT, Pfeiffer S, Ringelstetter L, Müller C, Zandkarimi F, Merl-Pham J, Bao X, Anastasov N, Kössl J, *et al*: GTP cyclohydrolase 1/tetrahydrobiopterin counteract ferroptosis through lipid remodeling. ACS Cent Sci 6: 41-53, 2020.
7. Mao C, Liu X, Zhang Y, Lei G, Yan Y, Lee H, Koppula P, Wu S, Zhuang L, Fang B, *et al*: DHODH-mediated ferroptosis defence is a targetable vulnerability in cancer. Nature 593: 586-590, 2021.
8. Dolma S, Lessnick SL, Hahn WC and Stockwell BR: Identification of genotype-selective antitumor agents using synthetic lethal chemical screening in engineered human tumor cells. Cancer Cell 3: 285-296, 2003.
9. Yang WS and Stockwell BR: Synthetic lethal screening identifies compounds activating iron-dependent, nonapoptotic cell death in oncogenic-RAS-harboring cancer cells. Chem Biol 15: 234-245, 2008.
10. Miotto G, Rossetto M, Di Paolo ML, Orian L, Venerando R, Roveri A, Vučković AM, Bosello Travain V, Zaccarin M, Zennaro L, *et al*: Insight into the mechanism of ferroptosis inhibition by ferrostatin-1. Redox Biol 28: 101328, 2020.
11. Hassannia B, Vandenabeele P and Vanden Berghe T: Targeting ferroptosis to iron out cancer. Cancer Cell 35: 830-849, 2019.
12. Lei G, Zhuang L and Gan B: Targeting ferroptosis as a vulnerability in cancer. Nat Rev Cancer 22: 381-396, 2022.
13. Kino T, Hurt DE, Ichijo T, Nader N and Chrousos GP: Noncoding RNA gas5 is a growth arrest- and starvation-associated repressor of the glucocorticoid receptor. Sci Signal 3: ra8, 2010.
14. Karreth FA, Tay Y, Perna D, Ala U, Tan SM, Rust AG, DeNicola G, Webster KA, Weiss D, Perez-Mancera PA, *et al*: In vivo identification of tumor-suppressive PTEN ceRNAs in an oncogenic BRAF-induced mouse model of melanoma. Cell 147: 382-395, 2011.
15. Tsai MC, Manor O, Wan Y, Mosammaparast N, Wang JK, Lan F, Shi Y, Segal E and Chang HY: Long noncoding RNA as modular scaffold of histone modification complexes. Science 329: 689-693, 2010.
16. Huarte M: The emerging role of lncRNAs in cancer. Nat Med 21: 1253-1261, 2015.
17. Zhang R, Pan T, Xiang Y, Zhang M, Xie H, Liang Z, Chen B, Xu C, Wang J, Huang X, *et al*: Curcumenol triggered ferroptosis in lung cancer cells via lncRNA H19/miR-19b-3p/FTH1 axis. Bioact Mater 13: 23-36, 2021.
18. Qin Y, Zhang D, Zhang H, Hou L, Wang Z, Yang L, Zhang M, Zhao G, Yao Q, Ling R and Zhang J: Construction of a ferroptosis-related five-lncRNA signature for predicting prognosis and immune response in thyroid carcinoma. Cancer Cell Int 22: 296, 2022.
19. Thai P, Statt S, Chen CH, Liang E, Campbell C and Wu R: Characterization of a novel long noncoding RNA, SCAL1, induced by cigarette smoke and elevated in lung cancer cell lines. Am J Respir Cell Mol Biol 49: 204-211, 2013.
20. Jiao Y, Li Y, Ji B, Cai H and Liu Y: Clinical value of lncRNA LUCAT1 expression in liver cancer and its potential pathways. J Gastrointestin Liver Dis 28: 439-447, 2019.
21. Chi J, Liu T, Shi C, Luo H, Wu Z, Xiong B, Liu S and Zeng Y: Long non-coding RNA LUCAT1 promotes proliferation and invasion in gastric cancer by regulating miR-134-5p/YWHAZ axis. Biomed Pharmacother 118: 109201, 2019.
22. Huan L, Guo T, Wu Y, Xu L, Huang S, Xu Y, Liang L and He X: Hypoxia induced LUCAT1/PTBP1 axis modulates cancer cell viability and chemotherapy response. Mol Cancer 19: 11, 2020.
23. Zhou Q, Hou Z, Zuo S, Zhou X, Feng Y, Sun Y and Yuan X: LUCAT1 promotes colorectal cancer tumorigenesis by targeting the ribosomal protein L40-MDM2-p53 pathway through binding with UBA52. Cancer Sci 110: 1194-1207, 2019.
24. Wang Y, Li Z, Li W, Zhou L and Jiang Y: Prognostic significance of long non-coding RNAs in clear cell renal cell carcinoma: A meta-analysis. Medicine (Baltimore) 98: e17276, 2019.
25. Shu X, Zhang Z, Yao ZY and Xing XL: Identification of five ferroptosis-related lncRNAs as novel prognosis and diagnosis signatures for renal cancer. Front Mol Biosci 8: 763697, 2022.
26. Xing XL, Yao ZY, Ou J, Xing C and Li F: Development and validation of ferroptosis-related lncRNAs prognosis signatures in kidney renal clear cell carcinoma. Cancer Cell Int 21: 591, 2021.
27. He Y, Ye Y, Tian W and Qiu H: A novel lncRNA panel related to ferroptosis, tumor progression, and microenvironment is a robust prognostic indicator for glioma patients. Front Cell Dev Biol 9: 788451, 2021.

28. Deng SH, Wu DM, Li L, Liu T, Zhang T, Li J, Yu Y, He M, Zhao YY, Han R and Xu Y: miR-324-3p reverses cisplatin resistance by inducing GPX4-mediated ferroptosis in lung adenocarcinoma cell line A549. Biochem Biophys Res Commun 549: 54-60, 2021.
29. Lei G, Zhang Y, Koppula P, Liu X, Zhang J, Lin SH, Ajani JA, Xiao Q, Liao Z, Wang H and Gan B: The role of ferroptosis in ionizing radiation-induced cell death and tumor suppression. Cell Res 30: 146-162, 2020.
30. Zhou Y, Zhou B, Pache L, Chang M, Khodabakhshi AH, Tanaseichuk O, Benner C and Chanda SK: Metascape provides a biologist-oriented resource for the analysis of systems-level datasets. Nat Commun 10: 1523, 2019.
31. Wang P, Guo Q, Qi Y, Hao Y, Gao Y, Zhi H, Zhang Y, Sun Y, Zhang Y, Xin M, *et al*: LncACTdb 3.0: An updated database of experimentally supported ceRNA interactions and personalized networks contributing to precision medicine. Nucleic Acids Res 50 (D1): D183-D189, 2022.
32. Li T, Chen B, Yang P, Wang D, Du B and Kang L: Long non-coding RNA derived from lncRNA-mRNA co-expression networks modulates the locust phase change. Genomics Proteomics Bioinformatics 18: 664-678, 2020.
33. Lin Y, Pan X and Shen HB: lncLocator 2.0: A cell-line-specific subcellular localization predictor for long non-coding RNAs with interpretable deep learning. Bioinformatics 37: 2308-2316, 2021.
34. Zhang X, Du L, Qiao Y, Zhang X, Zheng W, Wu Q, Chen Y, Zhu G, Liu Y, Bian Z, *et al*: Ferroptosis is governed by differential regulation of transcription in liver cancer. Redox Biol 24: 101211, 2019.
35. Gao R, Buechel D, Kalathur RKR, Morini MF, Coto-Llerena M, Ercan C, Piscuoglio S, Chen Q, Blumer T, Wang X, *et al*: USP29-mediated HIF1α stabilization is associated with sorafenib resistance of hepatocellular carcinoma cells by upregulating glycolysis. Oncogenesis 10: 52, 2021.
36. Karagkouni D, Paraskevopoulou MD, Tastsoglou S, Skoufos G, Karavangeli A, Pierros V, Zacharopoulou E and Hatzigeorgiou AG: DIANA-LncBase v3: Indexing experimentally supported miRNA targets on non-coding transcripts. Nucleic Acids Res 48 (D1): D101-D110, 2020.
37. Chen Y and Wang X: miRDB: An online database for prediction of functional microRNA targets. Nucleic Acids Res 48 (D1): D127-D131, 2020.
38. Livak KJ and Schmittgen TD: Analysis of relative gene expression data using real-time quantitative PCR and the 2(-Delta Delta C(T)) method. Methods 25: 402-408, 2001.
39. Yang WS, SriRamaratnam R, Welsch ME, Shimada K, Skouta R, Viswanathan VS, Cheah JH, Clemons PA, Shamji AF, Clish CB, *et al*: Regulation of ferroptotic cancer cell death by GPX4. Cell 156: 317-331, 2014.
40. Jiang L, Kon N, Li T, Wang SJ, Su T, Hibshoosh H, Baer R and Gu W: Ferroptosis as a p53-mediated activity during tumour suppression. Nature 520: 57-62, 2015.
41. Kwon MY, Park E, Lee SJ and Chung SW: Heme oxygenase-1 accelerates erastin-induced ferroptotic cell death. Oncotarget 6: 24393-24403, 2015.
42. Tian Y, Lu J, Hao X, Li H, Zhang G, Liu X, Li X, Zhao C, Kuang W, Chen D and Zhu M: FTH1 inhibits ferroptosis through ferritinophagy in the 6-OHDA model of Parkinson's disease. Neurotherapeutics 17: 1796-1812, 2020.
43. Dong H, Zhang C, Shi D, Xiao X, Chen X, Zeng Y, Li X and Xie R: Ferroptosis related genes participate in the pathogenesis of spinal cord injury via HIF-1 signaling pathway. Brain Res Bull 192: 192-202, 2023.
44. Cao Y, Luo F, Peng J, Fang Z, Liu Q and Zhou S: KMT2B-dependent RFK transcription activates the TNF-α/NOX2 pathway and enhances ferroptosis caused by myocardial ischemia-reperfusion. J Mol Cell Cardiol 173: 75-91, 2022.
45. Liu H, Zhang B, Chen S, Zhang Y, Ye X, Wei Y, Zhong G and Zhang L: Identification of ferroptosis-associated genes exhibiting altered expression in response to cardiopulmonary bypass during corrective surgery for pediatric tetralogy of fallot. Sci Prog 104: 368504211050275, 2021.
46. Koyanagi A, Kotani H, Iida Y, Tanino R, Kartika ID, Kishimoto K and Harada M: Protective roles of cytoplasmic $p21^{Cip1/Waf1}$ in senolysis and ferroptosis of lung cancer cells. Cell Prolif 55: e13326, 2022.
47. Deng H, Lin Y, Gan F, Li B, Mou Z, Qin X, He X and Meng Y: Prognostic model and immune infiltration of ferroptosis subcluster-related modular genes in gastric cancer. J Oncol 2022: 5813522, 2022.
48. Jehl A, Conrad O, Burgy M, Foppolo S, Vauchelles R, Ronzani C, Etienne-Selloum N, Chenard MP, Danic A, Dourlhes T, *et al*: Blocking EREG/GPX4 sensitizes head and neck cancer to cetuximab through ferroptosis induction. Cells 12: 733, 2023.
49. Ji HZ, Chen L, Ren M, Li S, Liu TY, Chen HJ, Yu HH and Sun Y: CXCL8 promotes endothelial-to-mesenchymal transition of endothelial cells and protects cells from Erastin-induced ferroptosis via CXCR2-mediated activation of the NF-κB signaling pathway. Pharmaceuticals (Basel) 16: 1210, 2023.
50. Sun K, Hou L, Guo Z, Wang G, Guo J, Xu J, Zhang X and Guo F: JNK-JUN-NCOA4 axis contributes to chondrocyte ferroptosis and aggravates osteoarthritis via ferritinophagy. Free Radic Biol Med 200: 87-101, 2023.
51. Ko J, Jang S, Kwon W, Kim SY, Jang S, Kim E, Ji YR, Park S, Kim MO, Choi SK, *et al*: Protective effect of GIP against monosodium glutamate-induced ferroptosis in mouse hippocampal HT-22 cells through the MAPK signaling pathway. Antioxidants (Basel) 11: 189, 2022.
52. Zhu L, Cao P, Yang S, Lin F and Wang J: Prolonged exposure to environmental levels of microcystin-LR triggers ferroptosis in brain via the activation of Erk/MAPK signaling pathway. Ecotoxicol Environ Saf 267: 115651, 2023.
53. Wang W, Zhu L, Li H, Ren W, Zhuo R, Feng C, He Y, Hu Y and Ye C: Alveolar macrophage-derived exosomal tRF-22-8BWS7K092 activates Hippo signaling pathway to induce ferroptosis in acute lung injury. Int Immunopharmacol 107: 108690, 2022.
54. Chen J, Chen Z, Yu D, Yan Y, Hao X, Zhang M and Zhu T: Neuroprotective effect of hydrogen sulfide subchronic treatment against TBI-induced ferroptosis and cognitive deficits mediated through Wnt signaling pathway. Cell Mol Neurobiol 43: 4117-4140, 2023.
55. Liu L, Wang M, Gong N, Tian P and Deng H: Se improves GPX4 expression and SOD activity to alleviate heat-stress-induced ferroptosis-like death in goat mammary epithelial cells. Anim Cells Syst (Seoul) 25: 283-295, 2021.
56. Niu B, Liao K, Zhou Y, Wen T, Quan G, Pan X and Wu C: Application of glutathione depletion in cancer therapy: Enhanced ROS-based therapy, ferroptosis, and chemotherapy. Biomaterials 277: 121110, 2021.
57. Matsui M and Corey DR: Non-coding RNAs as drug targets. Nat Rev Drug Discov 16: 167-179, 2017.
58. Chen X, Kang R, Kroemer G and Tang D: Broadening horizons: The role of ferroptosis in cancer. Nat Rev Clin Oncol 18: 280-296, 2021.
59. Qi L, Wang Y, Su S, Wang M, Jablonska E, Jia Y, Wang R, Hao S, Feng C, Li G, *et al*: Sodium selenite inhibits cervical cancer growth via ROS mediated AMPK/FOXO3a/GADD45a axis. Chem Biol Interact 367: 110171, 2022.
60. Zhang Y, Luo M, Cui X, O'Connell D and Yang Y: Long noncoding RNA NEAT1 promotes ferroptosis by modulating the miR-362-3p/MIOX axis as a ceRNA. Cell Death Differ 29: 1850-1863, 2022.
61. Wang S, Chen J, Li P and Chen Y: LINC01133 can induce acquired ferroptosis resistance by enhancing the FSP1 mRNA stability through forming the LINC01133-FUS-FSP1 complex. Cell Death Dis 14: 767, 2023.
62. Bhattacharjee S, Li J and Dashwood RH: Emerging crosstalk between long non-coding RNAs and Nrf2 signaling. Cancer Lett 490: 154-164, 2020.
63. Zhang L, Liu SK, Song L and Yao HR: SP1-induced up-regulation of lncRNA LUCAT1 promotes proliferation, migration and invasion of cervical cancer by sponging miR-181a. Artif Cells Nanomed Biotechnol 47: 556-564, 2019.
64. Wang X, Guo S, Zhao R, Liu Y and Yang G: STAT3-activated long non-coding RNA lung cancer associated transcript 1 drives cell proliferation, migration, and invasion in hepatoblastoma through regulation of the miR-301b/STAT3 axis. Hum Gene Ther 30: 702-713, 2019.
65. Wang L, Tang D, Wu T and Sun F: ELF1-mediated LUCAT1 promotes choroidal melanoma by modulating RBX1 expression. Cancer Med 9: 2160-2170, 2020.
66. Wang L, Xie Y, Wang J, Zhang Y, Liu S, Zhan Y, Zhao Y, Li J, Li P and Wang C: Characterization of a novel LUCAT1/miR-4316/VEGF-A axis in metastasis and glycolysis of lung adenocarcinoma. Front Cell Dev Biol 10: 833579, 2022.
67. Sun Y, Jin SD, Zhu Q, Han L, Feng J, Lu XY, Wang W, Wang F and Guo RH: Long non-coding RNA LUCAT1 is associated with poor prognosis in human non-small lung cancer and regulates cell proliferation via epigenetically repressing p21 and p57 expression. Oncotarget 8: 28297-28311, 2017.

68. Gutierrez-Cruz JA, Maldonado V and Melendez-Zajgla J: Regulation of the cancer stem phenotype by long non-coding RNAs. Cells 11: 2352, 2022.
69. Vierbuchen T, Agarwal S, Johnson JL, Galia L, Lei X, Stein K, Olagnier D, Gaede KI, Herzmann C, Holm CK, *et al*: The lncRNA LUCAT1 is elevated in inflammatory disease and restrains inflammation by regulating the splicing and stability of NR4A2. Proc Natl Acad Sci USA 120: e2213715120, 2023.
70. Tao Y, Liu Q, Wu R, Xiao C, Ni C, Wang K, Hu W, Zhong Z, Zhao J, Li Q, *et al*: Long noncoding RNA LUCAT1 enhances the survival and therapeutic effects of mesenchymal stromal cells post-myocardial infarction. Mol Ther Nucleic Acids 27: 412-426, 2021.
71. Zhang K, Wang Q, Zhong B and Gong Z: LUCAT1 as an oncogene in tongue squamous cell carcinoma by targeting miR-375 expression. J Cell Mol Med 25: 4543-4550, 2021.
72. Nai Y, Pan C, Hu X and Ma Y: LncRNA LUCAT1 contributes to cell proliferation and migration in human pancreatic ductal adenocarcinoma via sponging miR-539. Cancer Med 9: 757-767, 2020.
73. Liu Z, Gao H, Peng Q and Yang Y: Long noncoding RNA LUCAT1 promotes multiple myeloma cell growth by regulating the TGF-β signaling pathway. Technol Cancer Res Treat 19: 1533033820945770, 2020.
74. Mou E and Wang H: LncRNA LUCAT1 facilitates tumorigenesis and metastasis of triple-negative breast cancer through modulating miR-5702. Biosci Rep 39: BSR20190489, 2019.
75. Luzón-Toro B, Fernández RM, Martos-Martínez JM, Rubio-Manzanares-Dorado M, Antiñolo G and Borrego S: LncRNA LUCAT1 as a novel prognostic biomarker for patients with papillary thyroid cancer. Sci Rep 9: 14374, 2019.
76. Shen Q, Xu Z and Xu S: Long non-coding RNA LUCAT1 contributes to cisplatin resistance by regulating the miR-514a-3p/ULK1 axis in human non-small cell lung cancer. Int J Oncol 57: 967-979, 2020.
77. Han Z and Shi L: Long non-coding RNA LUCAT1 modulates methotrexate resistance in osteosarcoma via miR-200c/ABCB1 axis. Biochem Biophys Res Commun 495: 947-953, 2018.
78. Cronin SJF, Rao S, Tejada MA, Turnes BL, Licht-Mayer S, Omura T, Brenneis C, Jacobs E, Barrett L, Latremoliere A, *et al*: Phenotypic drug screen uncovers the metabolic GCH1/BH4 pathway as key regulator of EGFR/KRAS-mediated neuropathic pain and lung cancer. Sci Transl Med 14: eabj1531, 2022.
79. Sang L, Yang L, Ge Q, Xie S, Zhou T and Lin A: Subcellular distribution, localization, and function of noncoding RNAs. Wiley Interdiscip Rev RNA 13: e1729, 2022.
80. Li W, Pan T, Jiang W and Zhao H: HCG18/miR-34a-5p/HMMR axis accelerates the progression of lung adenocarcinoma. Biomed Pharmacother 129: 110217, 2020.
81. Hao R, Ge J, Song X, Li F, Sun-Waterhouse D and Li D: Cadmium induces ferroptosis and apoptosis by modulating miR-34a-5p/Sirt1axis in PC12 cells. Environ Toxicol 37: 41-51, 2022.